Nanoscale

RSC Publishing

PAPER

View Article Online
View Journal | View Issue

Cite this: *Nanoscale*, 2013, **5**, 7046

Controlled synthesis of ultrathin ZnO nanowires using micellar gold nanoparticles as catalyst templates†

Hong Yin,‡*[a] Qiushi Wang,[a] Sebastian Geburt,[b] Steffen Milz,[b] Bart Ruttens,[ac] Giedrius Degutis,[a] Jan D'Haen,[ac] Lianchen Shan,[a] Sathya Punniyakoti,[a] Marc D'Olieslaeger,[ac] Patrick Wagner,[ac] Carsten Ronning[b] and Hans-Gerd Boyen[ac]

We demonstrate a simple and effective approach to control the diameter of ultrathin ZnO nanowires with high aspect ratios and high densities over large areas. Diblock copolymer-based nanoparticle arrays exhibiting a high degree of hexagonal order and offering easy control of particle size (typically 1–10 nm) and interparticle spacing (25–150 nm) are utilized as nanocatalysts for the subsequent growth of semiconductor nanowires. The as-grown ZnO nanowires exhibit a single crystal hexagonal wurtzite structure and grow along the [0002] direction. Facetted catalyst particles were observed at the tip of the nanowires after synthesis, thus suggesting a catalyst-assisted vapor–solid–solid (VSS) rather than a vapor–liquid–solid (VLS) growth mechanism, the latter being frequently used in semiconductor nanowire production. Such a growth process allows us to easily prepare ultrathin ZnO nanowires with tunable diameters well below 10 nm by taking advantage of the inherent size control of the micellar method during deposition of the catalyst nanoparticles. Raman spectroscopy reveals a phonon confinement effect as the diameter of nanowires decreases. Photoluminescence spectra of these ultrathin nanowires indicate a blue shift of the free excitons and their phonon replicas by 37 meV induced by quantum confinement.

Received 22nd April 2013
Accepted 22nd May 2013

DOI: 10.1039/c3nr01938a

www.rsc.org/nanoscale

Introduction

Currently, quasi-one-dimensional nanostructures like semiconductor nanowires (NWs) are attracting strong attention[1] as they offer great potential to be exploited as advanced building blocks in, *e.g.*, nanoelectronics,[2] nanophotonics,[3] energy conversion,[4,5] bio/chemo-sensing,[6,7] or life science,[8] just to mention a few examples. The full exploration and, subsequently, exploitation of NWs make the precise control of their geometries (diameter, lateral position, *etc.*) during synthesis more and more indispensable thus triggering strong efforts to develop powerful (but still cheap) fabrication methods for this type of nanomaterial in current research. Zinc oxide (ZnO) is among the most promising systems for fabricating electronic and optoelectronic devices that can operate in the ultraviolet (UV) region owing to its direct band gap of 3.37 eV and the large exciton binding energy of 60 meV at room temperature.[9,10] Particularly, *ultrathin* ZnO NWs with diameters well below 10 nm are of high importance due to unique properties such as quantum confinement[10–13] which allow us to tailor electronic properties by means of the diameter of the NW.[14]

Several approaches to synthesize *ultrathin* ZnO NWs have been reported in the literature, which employ either physical/chemical vapor deposition[12,15,16] or wet chemical processes.[10,17,18] In contrast to vapor deposition methods, NWs synthesized *via* wet chemical processes generally exhibit low aspect ratios combined with a reduced crystal quality due to significantly lowered reaction temperatures. Hence, vapor deposition methods starting from nanoparticle catalysts become prevalent due to their high-throughput and easy fabrication combined with a high crystal quality. Gudiksen and Lieber proposed that the size of the catalyst nanoclusters determines the diameter of the resulting nanowires during growth.[19] Several catalyst template strategies such as metal colloids,[19] thickness-controlled metal thin films,[20] geometry-regulated electron-beam (E-beam) lithography,[21] patterned thin gold dots[15] and contact-printing processes[22] have been exploited since then to control the diameter of NWs. Some template approaches, though very successful in obtaining sub-10 nm diameter nanowires, involve rather complicated procedures such as soft lithography.[15]

[a]*Institute for Materials Research (IMO-IMOMEC), Hasselt University, Wetenschapspark 1, B-3590, Diepenbeek, Belgium. E-mail: hong.yin@uhasselt.be*

[b]*Institute for Solid State Physics, Friedrich-Schiller-University Jena, Jena, D-07743, Germany*

[c]*IMEC iwz, IMOMEC, Hasselt University, Wetenschapspark 1, B-3590, Diepenbeek, Belgium*

† Electronic supplementary information (ESI) available. See DOI: 10.1039/c3nr01938a

‡ Present address: State Key Lab of Superhard Materials, Jilin University, Changchun, 130012, P. R. China.

An alternative approach is based on the self-organization of diblock copolymers forming micellar nanoreactors in solution which finally can be transferred into well ordered arrays of size-selected catalyst particles on top of sufficiently flat substrates. This method has successfully been implemented for the growth of *ultrathin* Si NWs[23,24] *via* vapor–liquid–solid (VLS) growth. Simultaneously, strong efforts have been made to grow ZnO NWs by this technique due to their technological relevance.[25,26] In these experiments, a growth *via* VLS was observed with a minimum diameter of 20–30 nm which was supposed to represent a general limit for a given substrate material.[26]

Here, we will demonstrate that the micellar method can also be applied for the controlled synthesis of *ultrathin* ZnO nanowires with diameters well below 20 nm using tailored Au nanoparticle arrays for the catalyst-assisted growth. Such ultrathin NWs can be achieved with a narrow size distribution and high aspect ratio over large areas by exploiting the vapor–solid–solid (VSS) mechanism instead of the VLS process used before. In the VSS process, nanowires grow below the eutectic temperature T_E in contrast to the VLS mechanism which operates at temperatures above T_E. Therefore, slower growth rates are involved due to the weaker surface reactivity and/or lower diffusivity through the solid,[27–29] thus resulting in smaller nanowire diameters as compared to the VLS growth mode. Below, we present systematic studies of the obtained ultrathin ZnO NWs, which exhibit both phonon and quantum confinement effects, respectively. As the micellar technique allows us to prepare both elemental as well as alloy nanoparticles[30–33] as catalysts, its ability to produce hexagonally ordered arrays of size-selected nanoparticles with controllable interparticle spacing provides a promising pathway for diameter- and distance-controlled *ultrathin* nanowires not only for Si[23,24] and ZnO (this work), but also for many other material systems of interest.

Experimental

Ultrathin ZnO NWs were grown in a horizontal quartz tube (diameter 70 mm) inside a tube furnace. An alumina boat containing a mixture of ZnO (99.99%, Alfa Aesar) and graphite (99.99%, Alfa Aesar) powders (molar ratio 1 : 1) as source materials was stored at the center of the tube furnace. Si wafers (p-type) (decorated with Au nanoparticle arrays) were used as substrates, placed downstream from the center of the quartz tube in a temperature zone of about 450 °C. After evacuating the quartz tube down to 10^{-3} mbar, the furnace was heated up to 1050 °C at a rate of 50 °C min^{-1} under a constant flow (200 sccm) of Ar gas (6 N purity) and kept at high temperature for up to 180 min. The working pressure in the tube was in the range of about 10 mbar. After reaction, the furnace was cooled down to room temperature naturally.

Gold nanoparticle catalysts were prepared on top of silicon substrates (covered by a thin layer of natural silicon oxide) by exploiting micellar nanoreactors as intermediate template structures.[30,31] Briefly, this method is based on the self-organization of the diblock copolymer poly(styrene)-*block*-poly(2-vinylpyridine) [PS-*b*-P2VP] which forms reverse micelles within an apolar solvent like toluene when dissolved above the critical micellar concentration. After loading the polar core of such reverse micelles with a metal salt (here: $HAuCl_4$), a mono-micellar layer exhibiting a high degree of hexagonal order can be obtained on top of any flat substrate (metals, semiconductors, dielectrics) by means of an optimized dip-coating. Subsequently, the polymer matrix is removed by exposure to an isotropic oxygen plasma thereby inducing the formation of metal oxide nanoparticles which, however, can be reduced in an additional hydrogen plasma step into the pure metal. In the present case, the final result is an array of well-separated pure Au nanoparticles of rather uniform size which can easily be tuned between 1 and 10 nm diameter by means of the amount of metal salt added to the micellar solution. Additionally, the inter-particle spacing can be controlled between 25 and 150 nm by an appropriate choice of the individual block lengths of the polymers thereby preserving the high degree of hexagonal order of the mono-micellar layer (for more details, see ref. 30 and 31). Starting from such size-selected Au nanocatalysts, ultrathin ZnO NWs can finally be synthesized in a conventional tube furnace *via* a CVD process.

Atomic force microscopy (AFM, Park-NX10) and field emission scanning electron microscopy (FE-SEM, Philips FEI Quanta 200-FEG) were utilized to investigate the Au nanoparticles. The microstructure and morphology of the as-grown ZnO NWs were characterized using a FE-SEM, an X-ray diffractometer (XRD, Bruker D8 using a Cu Kα radiation) and a transmission electron microscope (TEM, Tecnai Spirit FEI). Raman spectra were acquired at room temperature using a Raman spectrometry system (Jobin-Yvon T64000) yielding a high spectral resolution less than 0.15 cm^{-1} and a 488 nm laser (Lexel SHG-95) as an excitation source. Photoluminescence (PL) measurements of the nanowire ensembles were conducted at $T = 4$ K using a 325 nm HeCd laser as an excitation source with an excitation power of 30 mW cm^{-2} and a LN_2 cooled CCD camera attached to a 500 nm monochromator as the detection system.

Results and discussions

Typical examples demonstrating the quality of the nanoparticle ensembles are given in Fig. 1(a)–(c) which display non-contact atomic force microscopy (AFM) images of the final arrangements of Au particles for the different micellar solutions used in the present study. Although not perfectly ordered, the particle arrays exhibit a high degree of hexagonal short range order with Gaussian size distributions of 3.1 ± 0.4 nm, 6.5 ± 0.6 nm, and 9.0 ± 0.8 nm (as derived from the corresponding particle size histograms) combined with average inter-particle spacings of 52 nm, 88 nm, and 108 nm, respectively.

Typical morphologies of as-prepared ZnO NWs are presented in Fig. 2. The low magnification scanning electron microscopy (SEM) image demonstrates NWs which have been uniformly grown with high areal density over macroscopic distances (Fig. 2a). The average diameter of the NWs is estimated to be around 16 nm when using 9 nm gold particles as catalysts. For this sample, a cross-sectional micrograph revealed an average length of approximately 3–4 μm resulting in a mean aspect ratio

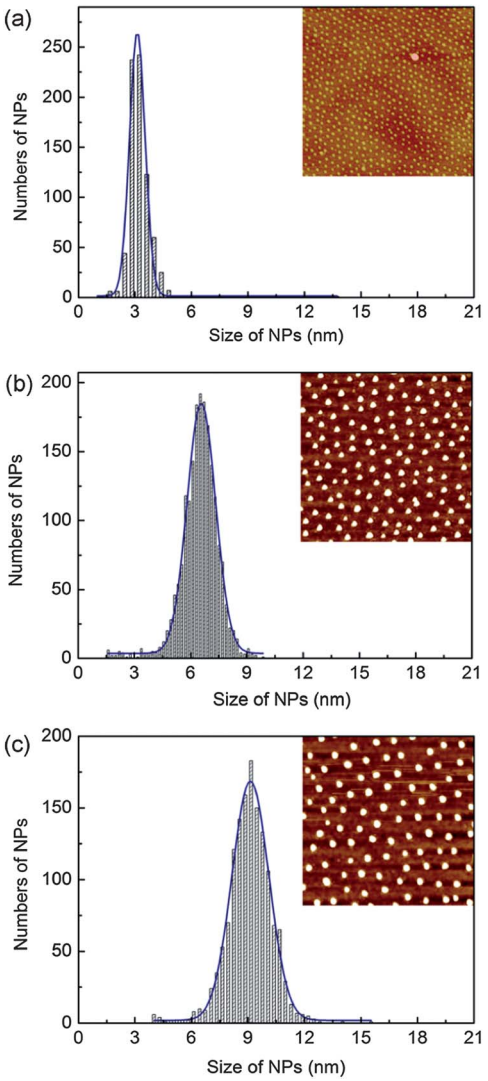

Fig. 1 AFM images and the corresponding size distributions of different arrays of Au NPs yielding 3.1 ± 0.4 nm (a), 6.5 ± 0.6 nm (b) and 9.0 ± 0.8 nm (c), respectively. All AFM images represent areas of 1 × 1 μm^2.

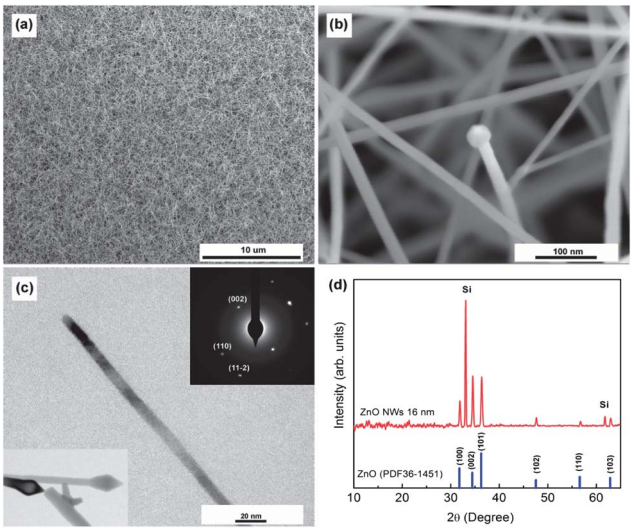

Fig. 2 Typical morphologies of ultrathin ZnO NWs: SEM images of (a) low magnification and (b) high magnification; (c) TEM results taken in bright field mode revealing facetted catalyst particles at the tip of the nanowires; the inset shows the electron diffraction pattern of the ZnO nanowire; (d) XRD pattern of as-synthesized ZnO NWs with an average diameter of 16 nm together with the reference pattern taken from the JCPDS card no. PDF36-1451.

of about 220, which is significantly higher than what has been reported for NWs synthesized *via* hydrothermal/solvothermal growth.[17,34] Fig. 2b displays a high magnification SEM image which uncovers a uniform and straight-line morphology with a smooth surface appearance of the ZnO NWs which are terminated by the catalyst particles at their ends. Often, in the case of catalyst-assisted synthesis, the growth of NWs is mediated by alloy/compound particles in the liquid phase (VLS mechanism)[35] which, when cooled down to room temperature after finishing the growth process, crystallize as smooth ellipsoids located at the tip (or root) of the wires. In our case, the particles after wire growth reveal planes, edges and corners at the tips of the nanowires (Fig. 2(b) and (c)), which allows us to identify the solid phase the particles remained during the growth, contradictory to the VLS mechanism.[27–29]

The prerequisite for VLS growth is a suitable solubility of the constituents of the growing nanowire within the catalyst particles, and a growth temperature above the eutectic temperature. Our growth temperature is around 450 °C, which lies well below the melting point of the bulk Au–Zn stoichiometric alloy (642 °C (ref. 36)). Meanwhile, it has to be pointed out that catalyst nanoparticles used in the present case most likely also have a reduced melting temperature with respect to the bulk material similar to their pure Au nanoparticle counterparts, but still remain in the solid regime.[37,38] Therefore, even though the results displayed above were based on post-synthesis analysis, it is likely that the starting Au nanoparticles and the subsequently formed particles at the wire tip remained solid during the entire growth process.

However, further measurements (Fig. S1 in the ESI†) on individual nanowires clearly show that the irregular particle at the tip consists of no Au, but only Zn and O similar to the wire body. The absence of Au in the finally remained catalyst particle might be due to the Au diffusion within or along the surface of the nanowires or evaporation due to a disordered, quasi-liquid surface formed in the nanometer regime.[39,40] Such reduction or depletion of Au catalyst particles has also been reported previously, although the exact pathways of Au atoms are still under discussion.[41–44]

Considering the fact that most of our nanowires end with apparently irregular particles, the surface diffusion induced nanowire growth mechanism could be possibly ruled out since the nanowires grown *via* surface diffusion usually have flat planes or significant tapering at the wire tips. It is worth noting that the way how the nanowires end up has been distinguished from other uncontrollable cases. With respect of the assistance of Au to the wire growth, the incoming Zn molecules evaporated from the ZnO/graphite source diffuse very quickly into Au, thus spontaneously forming Zn/Au alloy even at the low growth temperature (450 °C).[45] Here to simplify, the term "Zn/Au alloy"

will be used for the compound particles at the wire tips in the text. The size of alloy particles increases with the incorporation of Zn, until it reaches a limit when the Zn concentration is more than 90%. The oxidation of Zn occurs within the particles that generate the ZnO precipitates (nanowires). The formation of crystalline ZnO precipitates induced by internal oxidation has been already found in other binary systems, for instance, Zn–Ag and Zn–Cu.[46]

As can be inferred from the TEM image presented in Fig. 2c, the diameter of the obtained nanowires (about 16 nm) is larger than that of the precursor Au particles (about 9 nm), which is attributed to a volume increase upon formation of the (solid) intermetallic compound AuZn at the initial stage of the growth process.[38]

The crystal structure of these NWs was examined by means of electron diffraction (inset to Fig. 2c) as well as X-ray diffraction (Fig. 2d). In the latter case, the diffraction pattern of 16 nm thick wires can be indexed to the hexagonal wurtzite structure of ZnO according to the standard JCPDS (no. 36-1451) cards with lattice constants of $a = 0.325$ nm and $c = 0.521$ nm. No characteristic peaks arising from other crystal phases were observed. The electron diffraction pattern further confirms that the ZnO nanowires are monocrystalline and preferentially grow along the [0002] direction.

In order to establish the correlation between the catalyst size and the diameter of the resulting NWs, all different nanoparticle arrays presented in Fig. 1 were used for subsequent NW synthesis. It is important to note that well-isolated catalyst particles prepared by the micellar approach exhibit strong resistance against agglomeration as well as against Ostwald ripening even at temperatures approaching 1000 °C.[47] Thus, the small spread in particle size (Fig. 1) is expected to result in arrays of NWs with small variations in diameter thus providing a promising pathway for diameter-controlled NW synthesis. Fig. 3(a)–(c) show typical SEM images of the NW ensembles which have been synthesized starting from the respective Au NP arrays. The wire diameters were determined from several SEM images taken at different positions on each sample. Assuming Gaussian distributions, the resulting histograms allow us to extract average values for the diameter as 6 ± 1.8 nm, 10 ± 3 nm and 16 ± 4.5 nm when starting with the Au particle sizes of 3.1 ± 0.4 nm, 6.5 ± 0.6 nm and 9.0 ± 0.8 nm, respectively. After growth, the average diameters of the Zn/Au alloy particles at the tips are measured as 11.6 ± 2 nm, 17.7 ± 3 nm and 32 ± 6 nm, corresponding to their original counterpart. The detailed information is displayed in Fig. S2 and Table S1 in the ESI.† The diameters of all NWs are systematically smaller than the size of the particles at the tips, which in turn is larger than the size of the starting Au nanoparticles due to alloying of Zn and Au before nucleation of the nanowire occurs.[29,38] In order to better extract the controllability of such a growth process, the deviation of the Gaussian distribution of the nanowire and Zn/Au alloy particle systems has been systematically compared. For the 6 and 10 nm nanowires, the deviation of the Gaussian distribution mirrors that of the Zn/Au particles very well, suggesting that the dispersity of the wires is limited only by that of the Zn/Au particles. For the 16 nm diameter nanowires, a

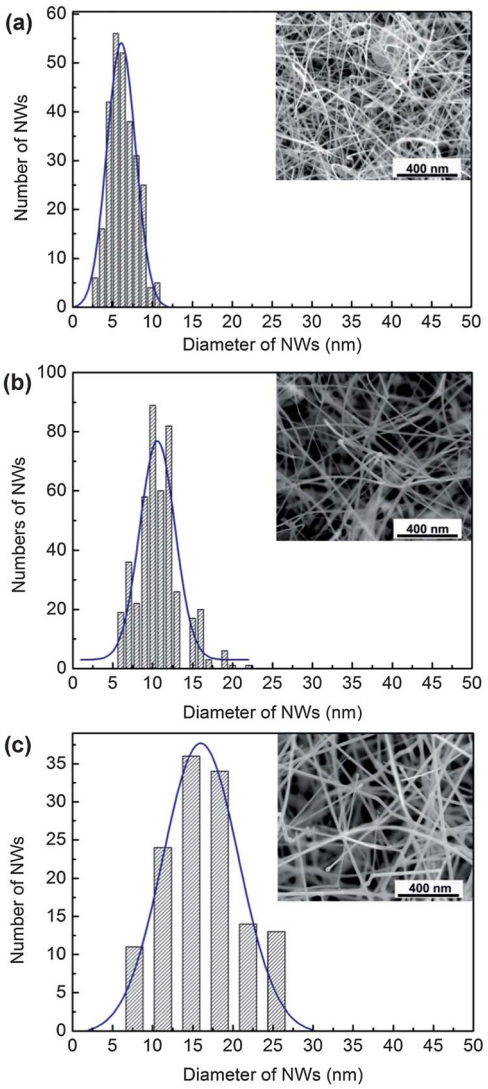

Fig. 3 SEM images and the corresponding distributions of ZnO NWs with average diameters of 6 ± 1.8 nm (a), 10 ± 3 nm (b), and 16 ± 4.5 nm (c), respectively. These wires were grown using the Au nanoparticle arrays shown in Fig. 1 as catalysts.

negligible difference of 1.5 nm is obtained as compared to the Zn/Au particle. Thus, it is reasonable to conclude that the diameter of nanowires is directly determined by the size of the compound particles during the growth, which is in turn dependent on the size of the starting Au catalyst nanoparticles when keeping other growth conditions constant. Furthermore, additional Au NPs with different size have also been exploited as nanocatalysts for tuning the diameter of ZnO NWs. Thus, the correlation between the catalyst size and resulting NW diameter is summarized in Fig. 4 suggesting a simple dependence between the two quantities. Consequently, ensembles of ZnO NWs with diameters well below 20 nm are available now, thus giving access to the investigation of their physical properties as described below.

Raman scattering, on one hand, is known to be a sensitive tool for the detection of disorder within a sample induced by, *e.g.*, composition fluctuations, impurities, or defects. On the

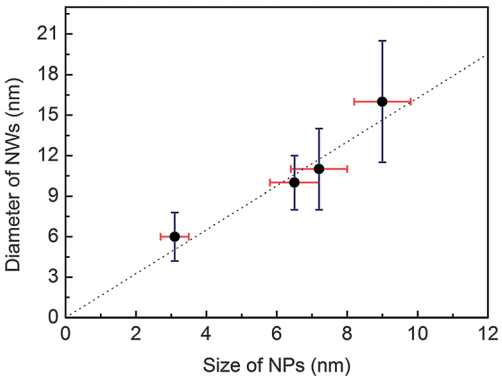

Fig. 4 Correlation between the size of the catalyst particles and the resulting diameter of the ultrathin ZnO NWs. The dotted line is a guide to the eyes.

other hand, it can also provide valuable information about size-induced effects of the system under investigation. For wurtzite ZnO, the phonon modes belonging to the E_2, E_1, and A_1 symmetries are Raman active. Consequently, six different Raman lines E_2 (high), E_2 (low), E_1 (TO), E_1 (LO), A_1 (TO) and A_1 (LO) could be present in a Raman spectrum depending on the experimental geometry. In the case of NW samples with random orientation, all modes were expected to be active. Fig. 5 presents the Raman scattering spectra of the samples presented before excitation by a 488 nm laser beam at room temperature. Besides the signal at 520 cm^{-1} which can be assigned to scattering by the Si(100) substrate,[48] a prominent peak is observed at about 438 cm^{-1} corresponding to the high frequency branch of the ZnO nonpolar optical phonon, E_2(high), thus representing one of the characteristic modes of wurtzite ZnO.[49,50] A weak but notable broad peak can be identified at about 580 cm^{-1} for nanowires with diameters $\leq$10 nm. It is most probably composed of the A_1 (LO) mode (574 cm^{-1}) and the E_1 (LO) mode (583 cm^{-1}) the latter being associated with oxygen deficiencies and zinc interstitials.[50] In contrast to bulk ZnO, no TO phonon modes (A_1 (TO) at 379 cm^{-1} and E_1 (TO) at 410 cm^{-1}) are detectable in the nonresonant Raman spectra as shown in Fig. 5 which is consistent with the earlier reports on ZnO NWs.[51]

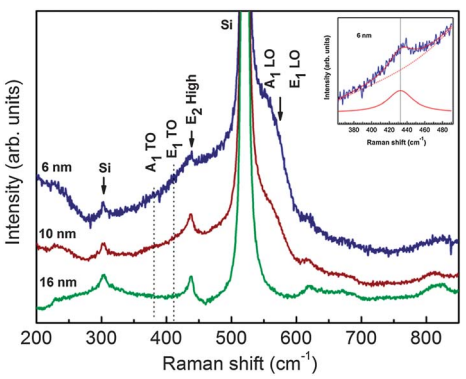

Fig. 5 Size dependent Raman spectra of ultrathin ZnO NWs with average diameters of 16 nm, 10 nm and 6 nm. The inset is a Lorentzian line shape which was fitted to the Raman experimental data of ZnO NWs with an average diameter of 6 nm.

The LO mode observed for NWs with small diameter might arise from local heating induced by the laser itself during operation. However, such possibility is very unlikely since (i) non-resonant Raman spectroscopy was used[52] and (ii) the 16 nm NWs do not show this specific mode despite identical experimental conditions during measurements. A more plausible explanation for the appearance of this mode for the smaller diameters is the presence of defects (*e.g.* oxygen vacancies) near the nanowire surface resulting in an enhanced line intensity due to larger surface-to-volume ratios in this diameter range.[53] The absence of the E_1 LO mode in the case of nanowires with an average diameter of 16 nm, on the other hand, clearly suggests that those nanowires are nearly free of defects and impurities and, thus, of high crystal quality.

The E_2 (high) mode is associated with the vibration of oxygen atoms within the crystal lattice.[54] Small frequency shifts of this mode have been attributed to phonon confinement induced by spatial boundaries, to phonon localization by defects, to laser-induced local heating and to the presence of internal stresses, as discussed for ZnO nanocrystals.[52] In order to derive at a more quantitative picture for our ZnO NWs, Lorentzian line shapes were fitted to the experimental data (see the inset to Fig. 5). As can be seen in Table 1, the E_2 mode exhibits a small but systematic redshift with respect to the bulk material as the wire diameter decreases. This redshift cannot be attributed to the presence of internal stresses, as mechanical stress induces blueshifts of the E_2 mode towards higher wavenumbers as found earlier.[55]

Laser-induced local heating as a reason for the observed redshift is also unlikely since nonresonant Raman spectroscopy was used in our studies.[51] Furthermore, changing the laser power did not result in any noticeable shift in the line position. As (i) the frequency shift of the E_2 line resulting from defects should be rather independent of the size of nanostructures[54] and (ii) confinement effects on LO or TO Raman bands are hard to be detected for nanowire diameters exceeding 10 nm,[56] the small redshift detected for NWs with 10 nm diameter (2 cm^{-1}) most likely represents the impact of defects, while the much more pronounced redshift observed for the thinnest NWs (6 cm^{-1}) is dominated by phonon confinement.

In order to further assess the quality of our ultrathin ZnO nanowires, their emission properties were investigated by photoluminescence (PL) measurements. Fig. 6(a) displays PL survey spectra for ZnO nanowire ensembles having diameters of 16 nm, 10 nm and 6 nm, respectively, together with results acquired on a ZnO nanowire ensemble with diameters in the range of 100–300 nm serving as a reference for nearly bulk like

Table 1 Frequencies (in units of cm^{-1}) and full width at half maximum (FWHM) of the Raman E_2 (high) mode for different nanowire diameters

Materials	Peak position [cm^{-1}]	FWHM [cm^{-1}]	Diameter [nm]
ZnO bulk[52,53]	439.0	—	—
ZnO NWs	437.8	10.3	16
ZnO NWs	437.0	11.2	10
ZnO NWs	432.9	21.6	6

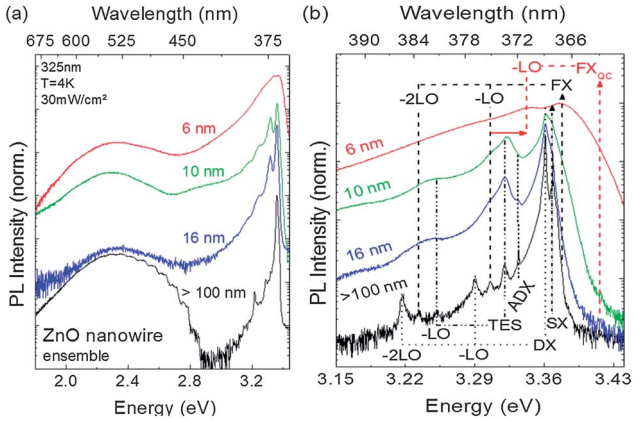

Fig. 6 (a) Low temperature PL spectra of ultrathin nanowires with average diameters of 16 nm, 10 nm and 6 nm together with results acquired on nanowires with a significantly larger diameter (>100 nm), the latter representing near-bulk behavior; (b) comparison of near-band-edge luminescence of ZnO nanowires as a function of their diameter.

emission properties. The prominent UV near band edge (NBE) emission can be observed in the range of 3.3 to 3.4 eV. It dominates the emission of all the samples with various diameters and can be attributed to the radiative recombination of free and bound excitons.[57] The weak deep-level (DL) green emission band centered at about 2.4 eV is assigned to exterior/interior related oxygen vacancies.[58,59] It is rather difficult to compare the absolute intensities of luminescence features, however, the strong NBE PL intensity compared to the DL emission implies also a high crystal quality of the synthesized ZnO nanowires.[60] In principle, reports in the literature usually claim that a higher surface-to-volume ratio as present in ZnO nanostructures might favor surface related defects, thus leading to an increase of the DL/NBE intensity ratio.[61] As seen in Fig. 6(a), such a behavior can indeed be recognized in the case of our ultrathin nanowires, with an intensity ratio of DL/NBE band gradually increasing with decreasing diameter in agreement with earlier work.[12]

Quantum confinement effects are expected in these nanoscaled entities when their size is approaching the exciton Bohr radius (ZnO $\sim$ 2.34 nm).[62] In fact, a blue shift of the excitonic emission has been found for ultrathin ZnO nanobelts and nanowire bundles for diameters less then 10 nm.[12,16,17] Thus, we compare the NBE luminescence features of ultrathin nanowires with those of the larger diameter nanowire sample, allowing us to make a concise evaluation of the size dependent properties. The details of the PL features related to the recombination of various excitons and their phonon replicas at 4 K are displayed in Fig. 6(b). For the nanowires with diameter larger than 100 nm, the emission line at 3.360 eV is dominating the spectra. This sharp emission peak is attributed to the neutral donor-bound exciton (DX) recombination.[57] The DX emission of the nanowires is accompanied by a shoulder at 3.367 eV, which is assigned to the recombination of excitons trapped at surface related states (SX).[63] At low temperatures, only a weak emission of the free exciton (FX) is observed as a shoulder at the higher energy side of the DX, because most of the excitons are localized at shallow donors.[64] In accordance with an earlier study,[12] emissions related to the FX and its first and second longitudinal optical (LO) phonon replicas can be clearly resolved at 3.377 eV, 3.305 eV and 3.233 eV respectively, which is consistent with bulk ZnO.[57] The energy difference between the lines and their phonon replicas is in good agreement with the energy of the LO phonon in ZnO (72 meV).[49] The small peak at around 3.333 eV, denoted as ADX, is associated with excitons bound to structural defects.[57] At 3.320 eV and 3.248 eV, the emission of a two-electron-satellite (TES) and its phonon replica can be observed, originating from donors which remain in an excited state after recombination of the bound exciton.[57]

The PL spectra of the ultrathin nanowires have been recorded at identical experimental conditions to the thicker nanowires. Their PL spectra are also dominated by the NBE luminescence arising from the free and bound exciton complexes; but the detailed excitonic features are not well resolved except for the strongest emission related to the DX line. As can be observed from Fig. 6(b), the PL intensity ratio of SX to DX is strongly size dependent since it increases dramatically with decreasing diameter, which is due to the increased surface-to-volume ratio. Furthermore, as can be recognized in Fig. 6(b), the FX line as well as its phonon replica are more prominent in the case of the ultrathin NWs as compared to ZnO NWs with average diameter larger than 100 nm. A new strong emission feature centered at 3.342 eV is observed for the nanowires of 6 nm diameter, which is strongly decreasing in intensity for thicker diameters. A similar emission was observed for ZnO nanowires with diameters below 10 nm previously[12] and has been attributed to the phonon replica of the free exciton (FX_{QC}-LO), which was blue shifted due to quantum confinement effects. As the diameter of the investigated nanowires is well below 10 nm, the assignment of the emissions to a quantum-confined free exciton (blue shifted by 37 meV) and its phonon replica appears reasonable. These effects can also be observed for the nanowires with 10 and 16 nm diameter, accompanied by an intensity which strongly decreases with increasing diameter.[11,16,17]

Conclusions

In conclusion, we have demonstrated an effective and simple route for the controlled synthesis of ultrathin ZnO NWs with tunable diameter, high areal density and high aspect ratio using micellar nanoparticles as catalyst templates. The diameter of the resulting nanowires can easily be adjusted to values well below 10 nm by proper control of the catalyst size. XRD and TEM consistently reveal wurtzite single crystals growing along the [0002] direction. SEM and TEM investigations unraveled a catalyst-assisted VSS growth mechanism which differs from the usually observed VLS mechanism. Raman measurements indicate phonon confinement effects for nanowires below 10 nm. Size-dependent PL spectra suggest that these ultrathin ZnO nanowires exhibit low defect concentrations and high optical quality. A blue shift of 37 meV has been observed for the nanowires with an average diameter of 6 nm at 4 K, implying the quantum confinement effect of the free exciton. Although

the micellar approach has demonstrated its great potential for the controlled deposition of ultrathin Si nanowires previously and ultrathin ZnO nanowires in this work, it can be expected that this technique should be applicable for the controllable synthesis of ultrathin semiconductor nanowires of other materials as well. Further investigations of *in situ* TEM are required to achieve structural and chemical information of interaction between the catalyst and nanowires during the growth as well as a better control of growth kinetics. Nevertheless, such an ability to precisely control the radial dimension of semiconductor nanowires in a regime where quantum confinement effects become increasingly important thus offers new opportunities to stimulate both fundamental as well as applied research in technologically important areas like, *e.g.*, nanoelectronics, optoelectronics, or bio/chemosensing.

Acknowledgements

This work was supported by the Research Foundation Flanders (FWO) within the Odysseus program and the Methusalem project 'NANO' as well as by the German Research Foundation (DFG) within the research unit FOR1616 (Ro1198). The authors are grateful for the technical support by J. Baccus (IMO, Hasselt University).

Notes and references

1 P. Yang, R. Yan and M. Fardy, *Nano Lett.*, 2010, **10**, 1529–1536.
2 Y. Cui, Z. Zhong, D. Wang, W. U. Wang and C. M. Lieber, *Nano Lett.*, 2003, **3**, 149–152.
3 M. H. Huang, S. Mao, H. Feick, H. Q. Yan, Y. Y. Wu, H. Kind, E. Weber, R. Russo and P. D. Yang, *Science*, 2001, **292**, 1897–1899.
4 Z. L. Wang and J. Song, *Science*, 2006, **312**, 242–246.
5 L. Baeten, B. Conings, H. G. Boyen, J. D'Haen, A. Hardy, M. D'Olieslaeger, J. V. Manca and M. K. Van Bael, *Adv. Mater.*, 2011, **23**, 2802–2805.
6 Y. Cui, Q. Q. Wei, H. K. Park and C. M. Lieber, *Science*, 2001, **293**, 1289–1292.
7 F. Patolsky, G. F. Zheng and C. M. Lieber, *Nat. Protoc.*, 2006, **1**, 1711–1724.
8 F. Patolsky, B. P. Timko, G. Yu, Y. Fang, A. B. Greytak, G. Zheng and C. M. Lieber, *Science*, 2006, **313**, 1100–1104.
9 X. Wang, C. J. Summers and Z. L. Wang, *Nano Lett.*, 2004, **4**, 423–426.
10 Y. Gu, I. L. Kuskovsky, M. Yin, S. O'Brien and G. F. Neumark, *Appl. Phys. Lett.*, 2004, **85**, 3833–3835.
11 M. Yin, Y. Gu, I. L. Kuskovsky, T. Andelman, Y. Zhu, G. F. Neumark and S. O'Brien, *J. Am. Chem. Soc.*, 2004, **126**, 6206–6207.
12 D. Stichtenoth, C. Ronning, T. Niermann, L. Wischmeier, T. Voss, C.-J. Chien, P.-C. Chang and J. G. Lu, *Nanotechnology*, 2007, **18**, 435701.
13 X. Xu, J. Zhuang and X. Wang, *J. Am. Chem. Soc*, 2008, **130**, 12527–12535.
14 H. Pan and Y. P. Feng, *ACS Nano*, 2008, **2**, 2410–2414.
15 E. C. Greyson, Y. Babayan and T. W. Odom, *Adv. Mater.*, 2004, **16**, 1348–1352.
16 X. Wang, Y. Ding, C. J. Summers and Z. L. Wang, *J. Phys. Chem. B*, 2004, **108**, 8773–8777.
17 F. Fang, D. Zhao, D. Shen, J. Zhang and B. Li, *Inorg. Chem.*, 2008, **47**, 398–400.
18 Y. W. Chen, Q. Qiao, Y. C. Liu and G. L. Yang, *J. Phys. Chem. C*, 2009, **113**, 7497–7502.
19 M. S. Gudiksen and C. M. Lieber, *J. Am. Chem. Soc.*, 2000, **122**, 8801–8802.
20 D. L. Guo, X. Huang, G. Z. Xing, Z. Zhang, G. P. Li, M. He, H. Zhang, H. Chen and T. Yu, *Phys. Rev. B: Condens. Matter Mater. Phys.*, 2011, **83**, 045403.
21 Y. J. Kim, C. H. Lee, Y. J. Hong, G. C. Yi, S. S. Kim and H. Cheong, *Appl. Phys. Lett.*, 2006, **89**, 163128.
22 S. H. Lee, G. Jo, W. Park, S. Lee, Y.-S. Kim, B. K. Cho, T. Lee and W. B. Kim, *ACS Nano*, 2010, **4**, 1829–1836.
23 J. Q. Lu and S. S. Yi, *Langmuir*, 2006, **22**, 3951–3954.
24 B. N. Mbenkum, A. S. Schneider, G. SchuÃàtz, C. Xu, G. Richter, P. A. van Aken, G. Majer and J. P. Spatz, *ACS Nano*, 2010, **4**, 1805–1812.
25 M. Haupt, A. Ladenburger, R. Sauer, K. Thonke, R. Glass, W. Roos, J. P. Spatz, H. Rauscher, S. Riethmuller and M. Moller, *J. Appl. Phys.*, 2003, **93**, 6252–6257.
26 A. Reiser, A. Ladenburger, G. M. Prinz, M. Schirra, M. Feneberg, A. Langlois, R. Enchelmaier, Y. Li, R. Sauer and K. Thonke, *J. Appl. Phys.*, 2007, **101**, 054319.
27 S. Kodambaka, J. Tersoff, M. C. Reuter and F. M. Ross, *Science*, 2007, **316**, 729–732.
28 V. Schmidt and U. Goesele, *Science*, 2007, **316**, 698–699.
29 D. S. Kim, R. Scholz, U. Goesele and M. Zacharias, *Small*, 2008, **4**, 1615–1619.
30 J. P. Spatz, S. Mossmer, C. Hartmann, M. Moller, T. Herzog, M. Krieger, H. G. Boyen, P. Ziemann and B. Kabius, *Langmuir*, 2000, **16**, 407–415.
31 G. Kastle, H. G. Boyen, F. Weigl, G. Lengl, T. Herzog, P. Ziemann, S. Riethmuller, O. Mayer, C. Hartmann, J. P. Spatz, M. Moller, M. Ozawa, F. Banhart, M. G. Garnier and P. Oelhafen, *Adv. Funct. Mater.*, 2003, **13**, 853–861.
32 H. G. Boyen, A. Ethirajan, G. Kastle, F. Weigl, P. Ziemann, G. Schmid, M. G. Garnier, M. Buttner and P. Oelhafen, *Phys. Rev. Lett.*, 2005, **94**, 016804.
33 A. Ethirajan, U. Wiedwald, H. G. Boyen, B. Kern, L. Y. Han, A. Klimmer, F. Weigl, G. Kastle, P. Ziemann, K. Fauth, J. Cai, R. J. Behm, A. Romanyuk, P. Oelhafen, P. Walther, J. Biskupek and U. Kaiser, *Adv. Mater.*, 2007, **19**, 406–410.
34 K. H. Tam, C. K. Cheung, Y. H. Leung, A. B. Djurisic, C. C. Ling, C. D. Beling, S. Fung, W. M. Kwok, W. K. Chan, D. L. Phillips, L. Ding and W. K. Ge, *J. Phys. Chem. B*, 2006, **110**, 20865–20871.
35 R. S. Wagner and W. C. Ellis, *Appl. Phys. Lett.*, 1964, **4**, 89–90.
36 ed. M. Hansen, *Series in Materials Science and Engineering*, 1v and 2 supp, McGraw-Hill, 1958.
37 P. Buffat and J. P. Borel, *Phys. Rev. A*, 1976, **13**, 2287–2298.
38 L. C. Campos, M. Tonezzer, A. S. Ferlauto, V. Grillo, R. Magalhaes-Paniago, S. Oliveira, L. O. Ladeira and R. G. Lacerda, *Adv. Mater.*, 2008, **20**, 1499–1504.

39 P. M. Ajayan and T. J. Marks, *Phys. Rev. Lett.*, 1989, **63**, 279–282.
40 W. Krakow, M. Jose-yacaman and J. L. Aragon, *Phys. Rev. B: Condens. Matter Mater. Phys.*, 1994, **49**, 591–596.
41 J. B. Hannon, S. Kodambaka, F. M. Ross and R. M. Tromp, *Nature*, 2006, **440**, 69–71.
42 D. S. Kim, R. Ji, H. J. Fan, F. Bertram, R. Scholz, A. Dadgar, K. Nielsch, A. Krost, J. Christen, U. Goesele and M. Zacharias, *Small*, 2007, **3**, 76–80.
43 D. S. Kim, U. Goesele and M. Zacharias, *J. Cryst. Growth*, 2009, **311**, 3216–3219.
44 L. Y. Cao, B. Garipcan, J. S. Atchison, C. Y. Ni, B. Nabet and J. E. Spanier, *Nano Lett.*, 2009, **6**, 1852–1857.
45 H. Yasuda and H. Mori, *Phys. Rev. Lett.*, 1992, **69**, 3747–3750.
46 W. P. Vellinga and J. T. M. Dehosson, *Acta Mater.*, 1997, **45**, 933.
47 F. Weigl, B. Koslowski and P. Ziemann, *Surf. Sci.*, 2008, **602**, 3714–3720.
48 J. H. Parker, D. W. Feldman and M. Ashkin, *Phys. Rev.*, 1967, **155**, 712.
49 T. C. Damen, S. P. S. Porto and B. Tell, *Phys. Rev.*, 1966, **142**, 570.
50 V. Pachauri, C. Subramaniam and T. Pradeep, *Chem. Phys. Lett.*, 2006, **423**, 240–246.
51 K. A. Alim, V. A. Fonoberov and A. A. Balandin, *Appl. Phys. Lett.*, 2005, **86**, 053103.
52 K. A. Alim, V. A. Fonoberov, M. Shamsa and A. A. Balandin, *J. Appl. Phys.*, 2005, **97**, 124313.
53 H.-M. Cheng, K.-F. Lin, H.-C. Hsu and W.-F. Hsieh, *Appl. Phys. Lett.*, 2006, **88**, 261909–261911.
54 K. F. Lin, H. M. Cheng, H. C. Hsu and W. F. Hsieh, *Appl. Phys. Lett.*, 2006, **88**, 263117.
55 G. W. Cong, H. Y. Wei, P. R. Zhang, W. Q. Peng, J. J. Wu, X. L. Liu, C. M. Jiao, W. G. Hu, Q. S. Zhu and Z. G. Wang, *Appl. Phys. Lett.*, 2005, **87**, 231903.
56 H. Richter, Z. P. Wang and L. Ley, *Solid State Commun.*, 1981, **39**, 625–629.
57 B. K. Meyer, H. Alves, D. M. Hofmann, W. Kriegseis, D. Forster, F. Bertram, J. Christen, A. Hoffmann, M. Strassburg, M. Dworzak, U. Haboeck and A. V. Rodina, *Phys. Status Solidi B*, 2004, **241**, 231–260.
58 K. Vanheusden, W. L. Warren, C. H. Seager, D. R. Tallant, J. A. Voigt and B. E. Gnade, *J. Appl. Phys.*, 1996, **79**, 7983–7990.
59 X. T. Zhang, Y. C. Liu, J. Y. Zhang, Y. M. Lu, D. Z. Shen, X. W. Fan and X. G. Kong, *J. Cryst. Growth*, 2003, **254**, 80–85.
60 M. Izaki, S. Watase and H. Takahashi, *Appl. Phys. Lett.*, 2003, **83**, 4930–4932.
61 I. Shalish, H. Temkin and V. Narayanamurti, *Phys. Rev. B: Condens. Matter Mater. Phys.*, 2004, **69**, 245401.
62 *Landolt-Börnstein-Group III*, ed. U. Rössler, 1999.
63 T. Voss, J. P. Richters and A. Dev, *Phys. Status Solidi B*, 2010, **247**, 2476–2487.
64 M. A. Zimmler, T. Voss, C. Ronning and F. Capasso, *Appl. Phys. Lett.*, 2009, **94**, 241120.